

# HELICOPTER VIBRATORY LOADS AND VIBRATIONS REDUCTION USING HIGHER-HARMONIC CONTROL

Aykut Tamer <sup>\*</sup>, Vincenzo Muscarello<sup>‡</sup>  
Pierangelo Masarati <sup>§</sup>, Giuseppe Quaranta <sup>†</sup>

Department of Aerospace Science and Technology,  
Politecnico di Milano, Milano - Italy

\* aykut.tamer@polimi.it  
† vincenzo.muscarello@polimi.it  
‡ pierangelo.masarati@polimi.it  
§ giuseppe.quaranta@polimi.it

Yavuz Yaman <sup>¶</sup>

Department of Aerospace Engineering,  
Middle East Technical University  
¶ yyaman@metu.edu.tr

## Abstract

This paper studies vibratory hub loads and cabin vibrations reduction using higher harmonic control. The dynamic analysis of the rotor is performed using a comprehensive analysis tool coupled with a gradient based optimization algorithm to evaluate the higher harmonic cyclic input which is expected to minimize vibratory hub loads. The hub force minimization problem is converted into a cabin vibration reduction problem using a comprehensive aeroservoelastic helicopter model which includes a linear time invariant aeroelastic rotor model, rigid and elastic fuselage modes, servo actuators and sensors for vibration measurement. The optimal higher harmonic control inputs are then applied and the accelerations are measured at the selected sensor locations and additionally aeroservoelastic stability analysis is performed. For the same aeroservoelastic model, a cabin vibration reduction procedure is formulated considering direct acceleration reduction at sensor locations. All studies are conducted on a light utility helicopter. Vibratory hub loads and sensor accelerations are presented and the differences in the objectives of minimum force at hub and minimum vibration at sensors are discussed.

## 1 INTRODUCTION

Helicopter vibrations are generally considered to limit several factors like safety, reliability, comfort and maximum speed. The aeroelastic interactions of the vehicle with the pilot are an additional source of degradation in handling qualities and safety [1–3] and chronic pain in long term [4]. Additionally, an excessive level of vibrations leads to an increase in maintenance stops which in turn increase the operational costs. More severe vibrations may cause failures and instability during flight leading to accidents. Therefore, the rotorcraft should be designed to achieve the lowest possible vibrational levels [5] which in turn reduce operation costs, increase reliability, improves passenger comfort and handling qualities, in other words improved acceptance for commercial market [6].

The benefits of vibration reduction are well known in rotorcraft industry since modern helicopters era started [7]. The techniques can be passive or active. The passive techniques do not require any actuation and aim at isolating the critical components from high levels of vibration,

hence in this case the vibratory loads are still present [8]. On the other hand the active techniques are implemented through on-board computers and servo actuators. The aim is directly to reduce oscillatory loads or their consequences rather than isolating them.

Higher Harmonic Control (HHC) is one of the active vibration reduction approaches currently implemented. It reduces the vibratory loads by exciting the swashplate at frequencies higher than fundamental frequency, which is the main rotor angular speed  $\Omega$  (known as (1/rev) in rotorcraft terminology) [9]. The main idea behind HHC is to smooth the rotor aerodynamics. A rotor with a number of  $N$  equally spaced identical blades acts as a filter when all the blade root loads are summed in the non-rotating reference frame. Hence only the loads at frequencies which are at integer ( $k$ ) multiples of the fundamental frequency multiplied by the blade number ( $kN/\text{rev}$ ) are transmitted to the fuselage [10]. Therefore the loads on the fuselage at  $N/\text{rev}$  frequency, the most critical one, can be reduced by moving the swashplate at the same frequency. This in turn induces blade pitch variations

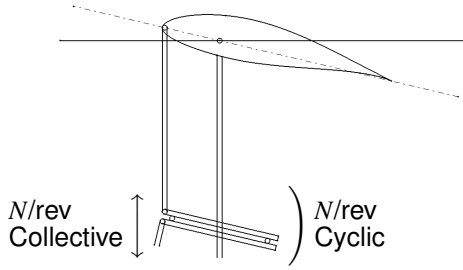


Figure 1: Schematic of HHC

that can smooth out aerodynamic loads. The principle is the same of regular 1/rev control actuation as given in Figure 1, but in this case higher harmonics are considered.

In the non-rotating frame there are six components for HHC input at  $n = N/\text{rev}$  harmonics. Then the contribution of HHC on the blade root motion  $\theta_{\Delta, BR}$  is summed to;

$$(1) \quad \theta_{\Delta, BR} = [\theta_{0,nc} \cos(n\psi) + \theta_{0,ns} \sin(n\psi)] \\ + [\theta_{lat,nc} \cos(n\psi) + \theta_{lat,ns} \sin(n\psi)] \cos(\psi) \\ + [\theta_{long,nc} \cos(n\psi) + \theta_{long,ns} \sin(n\psi)] \sin(\psi)$$

where  $\theta_{0,nc}$ ,  $\theta_{0,ns}$ ,  $\theta_{lat,nc}$ ,  $\theta_{lat,ns}$ ,  $\theta_{long,nc}$  and  $\theta_{long,ns}$  are independent of rotor azimuth angle  $\psi$  and applied in the fixed system [11]. The local blade root analysis is not within the scope of this study, therefore from now on HHC input  $\theta_{\Delta}$  refers to the vector of these six non-rotating frame inputs.

The HHC applications introduce weight penalties in terms of the servo actuators, hydraulics, computers and the additional necessity of local airframe strengthening which in turn degrades the aircraft performance. Additionally these systems are quite complex therefore the design, production, installation, certification and maintenance costs should also be taken into account [10]. Moreover reliability problems may arise since the HHC acts on the primary control chain. Because of these reasons, it is essential to estimate the possible reduction in vibrational level before implementing such systems. That evaluation of HHC performance provides the feasibility by comparing the benefits versus the weight and cost of the system. This study deals with the problem of evaluating the benefits which is the minimum vibrational level that can be achieved by HHC. The minimization can be performed on two objectives, either on the source of vibrations which is vibratory hub loads or the acceleration measurements at critical points on the fuselage. The former should be performed with an aeroelastic rotor model having proper trim

conditions since the loads are of aeroelastic origin. However due to the interactions with fuselage a detailed fuselage model gives more accurate results. On the other hand, in addition to rotor loads calculation, the second objective needs a more detailed model with an elastic fuselage representing all multiple load paths through the gearbox attachment and servo actuators that excite the fuselage.

It should be emphasized that HHC is usually implemented in adaptive manner. However this work focuses on setting up models that is capable of evaluating performance benefits of HHC application rather than a particular implementation. Therefore the algorithm of the HHC application is out of the scope of this work.

Considering the scope, paper is organized as follows. The following chapter introduces the method of the performance evaluation of HHC vibration reduction. The two objectives of HHC application are presented and the details of the analysis models are given. A model of a three-blade helicopter of the class of the Aerospatiale Gazelle is considered. After the method section, results of the numerical analysis are provided including vibratory loads and vibrations reduction at the sensors. The reduction in vibrations and the required HHC inputs are compared and discussed for each analysis.

## 2 METHOD

In this study, two objectives for helicopter vibration reduction are investigated for optimal HHC input. First, the hub loads induced by the main rotor are considered as objective such that the vibration reduction problem is solved by minimizing critical vibratory hub loads that are the sources of excitation. Then, in order to investigate the effect of HHC on fuselage vibrations, a more detailed linear time invariant (LTI) aeroservoelastic model is built using a comprehensive solver. Having the capability of assembling substructures from different sources, this model makes it possible to calculate the accelerations at selected points and allowing a comparison of the HHC performances at different cabin locations. The other objective for vibration reduction considers minimizing sensor accelerations at prescribed locations. For this purpose, a least squares approximation is formulated for an arbitrary number of vibration sensors and applied on the same LTI aeroservoelastic tool.

## 2.1 Minimum Vibratory Loads Optimization

The optimization problem is formulated as [12]

- (2) Find  $\mathbf{X} = \{x_1, x_2, \dots, x_m\}$  maximizing  $J(\mathbf{X})$   
subjected to  $\mathbf{g}(\mathbf{X}) \leq 0$  and  $\mathbf{l}(\mathbf{X}) = 0$ ,

where  $\mathbf{X}$  is termed as the design vector which includes  $m$  design variables,  $J(\mathbf{X})$  is called the objective function to be minimized,  $\mathbf{g}$  and  $\mathbf{l}$  are inequality and equality constraint vectors having arbitrary number of functions. The design variables are the model inputs that are the most sensitive to the optimization problem, the objective function is defined as the model output which is to be minimized and constraints are selected in order to prevent unrealistic results due to their dependence on design variables.

The objective of the optimization is to reduce critical  $N/\text{rev}$  loads originating from high frequency aerodynamics. Among them, the  $N/\text{rev}$  hub force component along the shaft, which is referred to as vertical hub force, is selected since the magnitude of vertical aerodynamic forces are higher than loads in other directions. The collective, longitudinal and lateral excitations of the swashplate in the non-rotating reference frame are determined as the design variables which are altered during the optimization analysis in order to minimize the objective function. For each collective, longitudinal and lateral excitation the amplitudes of sine and cosine components are required and this leads to six design variables.

It is not possible for an actuator to apply high values of HHC inputs due to power limits, hence the amplitudes of the selected design variables have been limited to below one degree. The change in blade pitch angle depends on the azimuthal location. Nevertheless, a maximum of one degree non-rotating frame input in a combination of collective longitudinal and lateral directions, gives the highest possible magnitude of 2.37 degrees variation at the blade root.

The other  $N/\text{rev}$  loads, which are not intended to be optimized, include two force and three moment components are limited based on the reference steady loads such that the  $N/\text{rev}$  loads are kept below 5% of those references. The reference for the longitudinal  $N/\text{rev}$  force component ( $F_x$ ) and lateral  $N/\text{rev}$  force component ( $F_y$ ) is determined as the helicopter weight. Similarly for the  $N/\text{rev}$  moment components, pitching ( $M_y$ ), rolling ( $M_x$ ) and yawing ( $M_z$ ), the reference is determined as the main rotor torque at the analyzed flight speed. Apart

from these inequality constraints ( $\mathbf{g}(\mathbf{X})$ ), no equality constraint ( $\mathbf{l}(\mathbf{X})$ ) is defined.

The calculation of vibratory loads needs comprehensive analysis tools. For this purpose CAMRAD/JA is selected [13]. The required higher harmonic control analysis are performed at free flight trim for an aeroelastic rotor, rigid fuselage having 6 degrees of freedom, rigid tail rotor and stability derivatives for vertical and horizontal stabilizers. This CAMRAD model is coupled with CONMIN gradient based optimization algorithm [14] so that the HHC inputs on the swashplate that can minimize the critical vibratory hub loads, are evaluated.

The flowchart of the coupling between CONMIN and CAMRAD/JA is given in Figure 2. The vectors represent design variables ( $\mathbf{X}$ ), objective function ( $J(\mathbf{X})$ ) and constraint function ( $\mathbf{g}(\mathbf{X})$ ). The role of the comprehensive model in this process is to provide the values of objective function and constraints for the assigned design variables. After the CAMRAD/JA model is initialized and CONMIN inputs ( $J(\mathbf{X}), \mathbf{g}(\mathbf{X})$ ) and outputs ( $\mathbf{X}$ ) are defined, the optimization routine accepts initial design variables ( $\mathbf{X}_0$ ) and computes the initial value of objective function ( $J(\mathbf{X}_0)$ ). This is essentially due to the fact that the optimization algorithm is gradient based. In the optimization routine, CONMIN provides the design variables to CAMRAD/JA based on the evaluation of the derivatives of objective function and constraint functions, whereas CAMRAD supports CONMIN by calculating these functions. This calculation continues until all the finite difference derivatives of  $J(\mathbf{X})$  and  $\mathbf{g}(\mathbf{X})$  are evaluated for all design variables ( $\mathbf{X}$ ). Based on the derivatives CONMIN assigns the new set of design variables giving maximum gradient in objective function  $\max(\Delta J(\mathbf{X}_i)/\Delta \mathbf{X}_i)$  while satisfying constraints. This loop iterates until convergence.

## 2.2 LTI Aeroservoelastic Model for Vibration Reduction Analysis

The second objective, which is vibration reduction analysis including elastic fuselage, servo actuators and sensors for vibration calculation, is performed using a simulation tool called MASST (Modern Aeroservoelastic State Space Tools) which has been developed at Politecnico di Milano for the aeroservoelastic and aeromechanical analysis of aircraft and rotorcraft [15, 16]. MASST analyzes compact yet complete modular models of complex linearised aeroservoelastic systems. Models are not directly formulated in MASS; they

**Definitions**  
 $\mathbf{X}$  = Design Variables Vector  
 $J(\mathbf{X})$  = Objective Function  
 $\mathbf{g}(\mathbf{X})$  = Inequality Constraint Vector

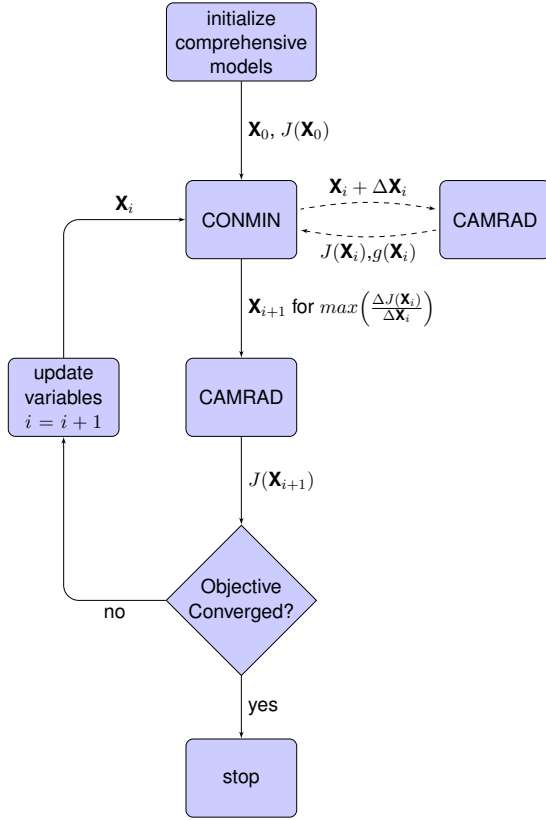


Figure 2: CONMIN-CAMRAD Coupling

are rather composed of subcomponents collected from well-known, reliable and possibly state-of-the-art sources and blended together in a mathematical environment.

The problem is formulated in state-space form. This approach is often termed “modern” in the automatic control community. The equations of motion of the system are cast as first order time differential equations. As a consequence, generic state-space approaches can be used to analyze aeroelastic systems.

MASST has been designed to be modular and to incorporate heterogeneous subcomponents from different sources to model:

1. deformable aircraft structural dynamics;
2. airframe unsteady aerodynamics;
3. rotor aeroelasticity;
4. drive train dynamics;

5. servoactuators dynamics;
6. sensors and filters dynamics;
7. (Automatic) Flight Control System (FCS);
8. pilot biomechanics.

When these elements are combined, they provide a powerful and flexible closed loop aeroservoelastic modeling capability.

Each component is modeled in its most natural and appropriate modeling environment and then cast into state-space form. Substructures are connected using the Craig-Bampton Component Mode Synthesis (CMS) approach [17].

### 2.2.1 Rotor Aeroelasticity Subproblem

From the point of view of the interaction with the rest of the vehicle, the Main Rotor (MR) contribution is expressed in terms of a LTI aeroelastic operator. For a given steady flight condition, relates forces and moments produced by the rotor at the MR attachment point,  $\mathbf{f}_{MR}$ , to the components of motion at that point (displacements and rotations),  $\mathbf{x}_{MR}$ , and to the MR controls, including regular trim control (1/rev) and any harmonic input ( $N/rev$ ),  $\delta_{MR} = \{\theta_0; \theta_{1c}; \theta_{1s}; \theta_{Nc}; \theta_{Ns}\}$ , namely

$$(3) \quad \mathbf{f}_{MR} = \mathbf{H}_{xMR}(j\omega)\mathbf{x}_{MR} + \mathbf{H}_{\delta MR}(j\omega)\delta_{MR} + \mathbf{f}_{N/rev};$$

$\mathbf{f}_{N/rev}$  are  $N/rev$  excitation forces and moments generated by the rotor aerodynamics. Note that the rotation components of the motion include both rigid-body motion and deformation effects of the airframe.

In practice, these loads are evaluated in the frequency domain for a set of discrete frequencies and for a given set of trim points, ranging from hover to forward flight at different speeds. In this study CAMRAD JA is used both in optimization and detailed aeroservoelastic analysis. In the detailed aeroservoelastic analysis the LTI model is combined to the fuselage. Since this LTI rotor model does not include harmonic loads, the  $N/rev$  force and moments at the rotor hub obtained from CAMRAD JA are implemented as an external force and moment input in MASST model.

### 2.2.2 Airframe Dynamics Problem

The structural dynamics model simply consists of the second-order equations of the rigid-body and flexible airframe dynamics,

$$(4) \quad \mathbf{M}\ddot{\mathbf{q}} + \mathbf{C}\dot{\mathbf{q}} + \mathbf{K}\mathbf{q} = \mathbf{f},$$

formulated for the generalized coordinates  $\mathbf{q}$ . The motion of the MR attachment point is known in terms of the corresponding modal displacements  $\mathbf{x}_{MR} = \mathbf{U}_{MR}\mathbf{q}$ . As a consequence, the frequency domain representation of the airframe dynamics is simply coupled to the MR aeroelastic model using the Principle of Virtual Work (PVW), namely

$$(5) \quad \begin{aligned} \delta \mathcal{W}_{MR} &= \delta \mathbf{x}_{MR}^T \mathbf{f}_{MR} \\ &= \delta \mathbf{q}^T \mathbf{U}_{MR}^T (\mathbf{H}_{xMR}(j\omega) \mathbf{U}_{MR} \mathbf{q} \\ &\quad + \mathbf{H}_{\delta MR}(j\omega) \boldsymbol{\delta}_{MR} + \mathbf{H}_{qf}(j\omega) \mathbf{f}_{N/rev}), \end{aligned}$$

which contributes to 4, yielding

$$(6) \quad \begin{aligned} &(-\omega^2 \mathbf{M} + j\omega \mathbf{C} + \mathbf{K} - \mathbf{U}_{MR}^T \mathbf{H}_{xMR}(j\omega) \mathbf{U}_{MR}) \mathbf{q} \\ &= \mathbf{U}_{MR}^T \mathbf{H}_{\delta MR}(j\omega) \boldsymbol{\delta}_{MR} + \mathbf{U}_{MR}^T \mathbf{H}_{qf}(j\omega) \mathbf{f}_{N/rev} \end{aligned}$$

As long as all the controls  $\boldsymbol{\delta}$  and  $N/rev$  excitation loads  $\mathbf{f}_{N/rev}$  are considered, including for example also the collective pitch of the tail rotor  $\delta_{TR}$ , i.e.  $\boldsymbol{\delta} = \{\boldsymbol{\delta}_{MR}; \delta_{TR}\}$ , the problem can be written as

$$(7) \quad \mathbf{q} = \mathbf{H}_{q\delta}(j\omega) \boldsymbol{\delta} + \mathbf{H}_{qf}(j\omega) \mathbf{f}_{N/rev},$$

where additional exogenous inputs and disturbances are neglected, since the analysis focuses on harmonic loads.

In order to introduce HHC inputs and also account for the load path through servos, actuator dynamics are considered as well. The dynamic relationship between the command requested by the pilot and the actual motion prescribed to the controls is

$$(8) \quad \boldsymbol{\delta} = \mathbf{H}_{act}(j\omega) \boldsymbol{\eta} + \mathbf{H}_{dc}(j\omega) \mathbf{f}_{act},$$

where vector  $\boldsymbol{\eta}$  contains the motion of the control inceptors, while  $\mathbf{f}_{act}$  represents the force transmitted by the actuators;  $\mathbf{H}_{dc}(j\omega)$ , the dynamic compliance of the actuator, is often neglected or statically approximated. Usually, a first- or second-order equation is considered for the actuator dynamics transfer function  $\mathbf{H}_{act}(j\omega)$ . In this study rigid actuators are connected to the rotor at their usual rotor connection and rigidly attached to the fuselage at their fuselage connection. This ignores the link to the pilot and servos act as a secondary load path to fuselage.

MASST requires the mode shapes and modal mass matrix of the fuselage to model the rigid and elastic behavior of the airframe. For this purpose a stick model, which uses an original 3 node linearized finite volume beam formulation together with lumped inertia and rod models [18, 19], is used to approximate the fuselage structural dynamics. The complete MASST aeroservoelastic

model, composed of airframe stick model, servo actuators, main rotor and acceleration sensors, is given in Figure 3.

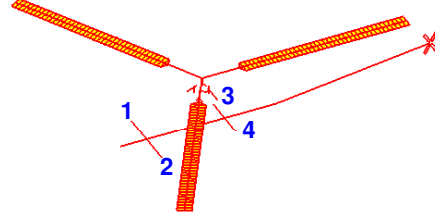


Figure 3: Helicopter Model in MASST

There are 6 beam elements on the longitudinal axis which models cabin and tail boom. There is also one node at rotor hub. The main rotor, tail rotor, gear box and engine are considered as lumped masses and inertias. The lateral extensions on the fuselage longitudinal axis, labeled 1, 2, 3, 4 in Figure 3, are four sensor locations where accelerations are measured. These sensors can be placed anywhere in the fuselage such as pilot/passenger seats, avionics and transmission locations, depending on the objective of vibration analysis. In this model, four sensors are used as given in Table 1 assuming that sensors 1 and 2 loosely correspond to crew seat locations and sensors 3 and 4 are given as arbitrary locations near transmission. In the present analysis, the sensors are attached to the nearest longitudinally aligned beam node and their contribution to mode shapes is calculated by considering a rigid link in-between.

Table 1: Sensor Locations (m.) with respect to rotor hub

Sensor #	x(+ aft)	y (+ right)	z (+ up)
1	-1.42	0.8	-1.52
2	-1.42	-0.8	-1.52
3	0.58	0.6	-1.52
4	0.58	-0.6	-1.52

In order to attach the rotor to the fuselage and transfer loads and motion, a gear box attachment is necessary. A gearbox attachment, as shown in Figure 4, has been modeled to gain the capability to address this component in the LTI analysis with the future objective of exploiting its compliance to introduce passive and active vibration suppression capabilities. The 4 rods, having high stiffness, connect the main rotor to the fuselage and are mainly responsible for supporting and transferring vertical force and pitching and rolling moments. There

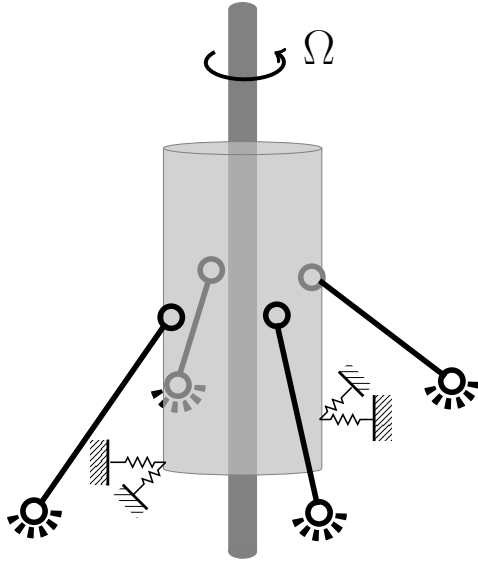


Figure 4: Gearbox Support

are two groups of bushings, composed of two perpendicular elements, located parallel to the main rotor plane at the bottom of the gearbox attachment. Therefore the role of the 4 bushings is to support and transfer forces and moments in the rotor plane, namely, longitudinal and lateral forces and yawing moment. These elements each having 2 nodes is connected to the main rotor at one node and to the fuselage at the other node. As in the case of the sensors, the motion contribution of the gearbox attachment node is calculated by attaching them to the nearest rotor/fuselage node and evaluating their motion assuming a rigid link between the gearbox attachment nodes and the corresponding rotor/fuselage node.

The fuselage stick model uses six rigid body modes and four elastic modes whose frequencies are within  $N/\text{rev}$  and slightly above. Due to the lack of detailed mass and stiffness data, mass and elasticity distributions are assumed to obtain natural frequency values as close as possible to those of the original work [20]. Modal damping of 2% is assumed. The comparison is given in Table 2 and the corresponding mode shapes are plotted in Figure 5. It is important to note that the  $N/\text{rev}$  frequency (with  $N = 3$ ,  $3/\text{rev} = 19.35$  Hz) is between the 3rd and the 4th structural modes.

### 2.3 Cabin Vibration Calculation

Having completed the LTI aeroservoelastic model, the vibrations at the sensor locations can

Table 2: Structural Bending (B.) and Torsion (T.) Modes of the Fuselage for Reference (R.) and Stick Model (S.M.) and % difference ( $\Delta$ )

Mode	R. [20]	S.M.	$\Delta$
1st Vertical B.	7.96	7.59	-5%
1st Lateral B.	9.99	10.21	+2%
1st Fuselage T.	17.59	18.08	+3%
2nd Vertical B.	20.93	21.10	+1%

be found using state the space form of the MASST model. Figure 6 provides a simple representation. The loads coming from the HHC actuation ( $F_{H,\Delta\theta}$ ), rotor feedback ( $F_{H,a_H}$ ) and  $N/\text{rev}$  loads prior to HHC ( $F_{H,N/\text{rev}}$ ) actuation are summed at the hub and excite the fuselage through the gearbox attachment and servos. The output accelerations ( $a_S$ ) are evaluated using the transfer function from the hub forces to the sensor accelerations ( $H_{a_S,F_H}$ ). Moreover, the importance of a coupled rotor fuselage model can be seen from the load feedback ( $F_{H,a_H}$ ) arising because of the rotor response to hub acceleration ( $a_H$ ).

### 2.4 Least Squares Formulation for Minimum Fuselage Vibration

The least squares solution is formulated for an acceleration vector ( $\mathbf{y}$ ) with arbitrary number of sensors and HHC swashplate actuation vector ( $\theta_\Delta = \theta_{\text{HHC}}$ ). The problem is formulated in the frequency domain, such that real and imaginary parts of the solution directly represent the cosine and sine terms of the control input. First a scalar objective function is written using a weighted multiplication of  $\mathbf{y}$  and  $\theta_\Delta$  with their complex conjugate transposes (Hermitian),  $\mathbf{y}^H$  and  $\theta_\Delta^H$ ;

$$(9) \quad J = \mathbf{y}^H \mathbf{W} \mathbf{y} + \theta_\Delta^H \mathbf{R} \theta_\Delta$$

where  $\mathbf{W}$  and  $\mathbf{R}$  are weighting matrices for acceleration and HHC input vectors respectively. The matrix  $\mathbf{W}$  is defined depending on the priority of sensor locations. If the accelerations at all the sensors are aimed to be minimized to the same extent then  $\mathbf{W}$  is an identity matrix with the dimension of number of sensors. However, in many applications minimizing accelerations everywhere is not practical and moreover some locations in the cabin such as the pilot seat have higher priority compared to other locations. In this case the elements of  $\mathbf{W}$  would have different values depending of their importance.

In order to find the minimum,  $J$  is differentiated

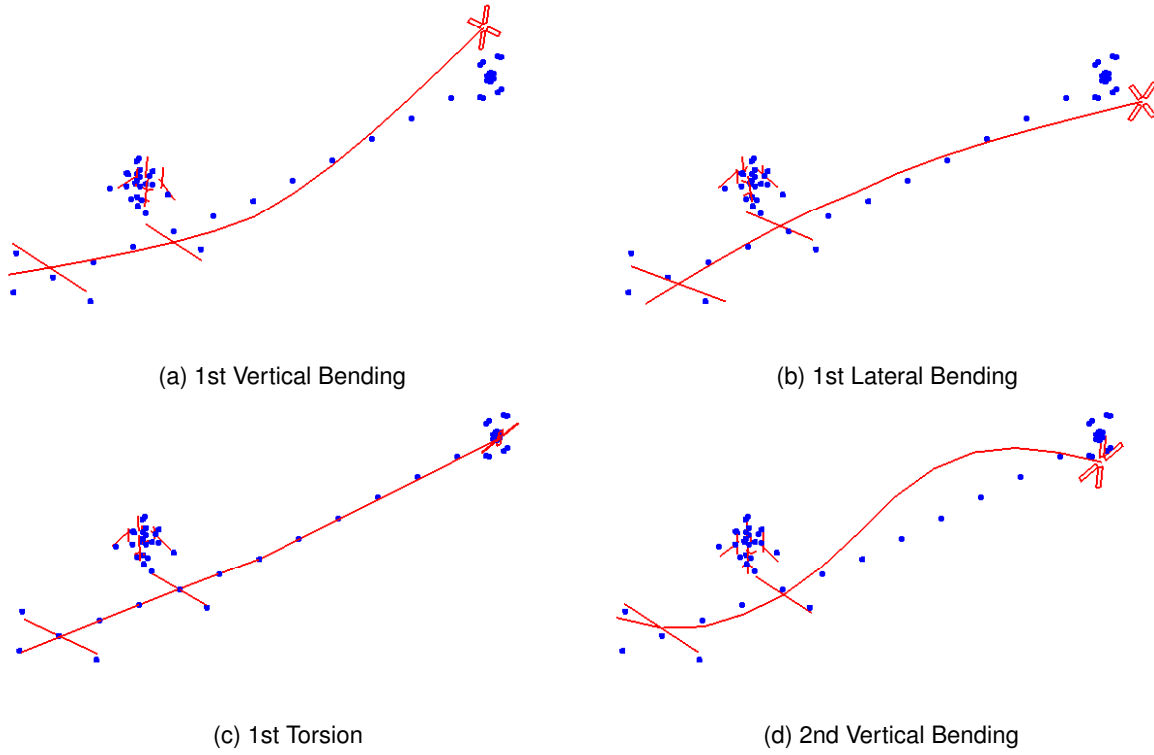


Figure 5: Elastic Degrees of Freedom of the Fuselage

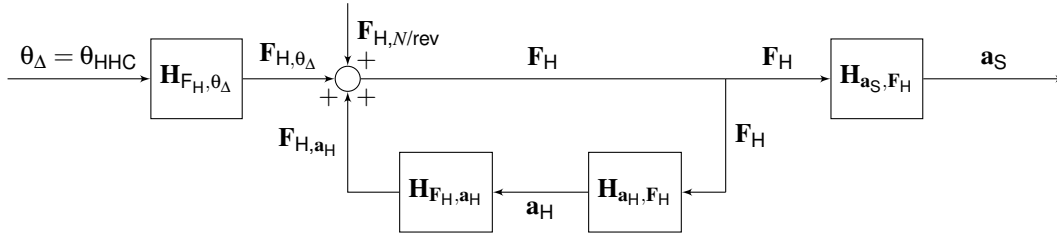


Figure 6: Block diagram representation of HHC vibration reduction problem in MASST

with respect to  $\theta_{\Delta}^H$  and equated to zero which gives;

$$(10) \quad \frac{\partial J}{\partial \theta_{\Delta}^H} = 0 \Rightarrow \frac{\partial y^H}{\partial \theta_{\Delta}^H} \mathbf{W} \mathbf{y} + \mathbf{R} \theta_{\Delta} = 0$$

The acceleration  $\mathbf{y}$  can be derived from state space representation of the aeroservoelastic model which can be stated with a participation in force and HHC inputs as

$$(11) \quad \begin{aligned} \dot{\mathbf{x}} &= \mathbf{A} \mathbf{x} + \mathbf{B}_f \mathbf{f} + \mathbf{B}_{\theta_{\Delta}} \theta_{\Delta} \\ \mathbf{y} &= \mathbf{C} \mathbf{x} + \mathbf{D}_f \mathbf{f} + \mathbf{D}_{\theta_{\Delta}} \theta_{\Delta} \end{aligned}$$

where  $\mathbf{f}$  is the forcing term and  $\mathbf{x}$  is the state vector of the system. For harmonic excitation, the state vector is written as,

$$(12) \quad \mathbf{x} = (j\omega \mathbf{I} - \mathbf{A})^{-1} (\mathbf{B}_f \mathbf{f} + \mathbf{B}_{\theta_{\Delta}} \theta_{\Delta})$$

For our problem  $\omega$  is the  $N/rev$  frequency. Inserting Eq. (12) into the acceleration relation of Eq. (11), the acceleration vector can be obtained as,

$$(13) \quad \mathbf{y} = \mathbf{H}_f \mathbf{f} + \mathbf{H}_{\theta_{\Delta}} \theta_{\Delta}$$

where  $\mathbf{H}_f$  and  $\mathbf{H}_{\theta_{\Delta}}$  are the transfer functions from forcing input and HHC input respectively.

$$(14) \quad \begin{aligned} \mathbf{H}_f &= \mathbf{C}(j\omega \mathbf{I} - \mathbf{A})^{-1} \mathbf{B}_f + \mathbf{D}_f \\ \mathbf{H}_{\theta_{\Delta}} &= \mathbf{C}(j\omega \mathbf{I} - \mathbf{A})^{-1} \mathbf{B}_{\theta_{\Delta}} + \mathbf{D}_{\theta_{\Delta}} \end{aligned}$$

Now the derivative of  $\mathbf{y}^H$  can also be written as

$$(15) \quad \frac{\partial \mathbf{y}^H}{\partial \theta_{\Delta}^T} = \mathbf{H}_{\theta_{\Delta}}^H$$

And finally combining Eqs. (9), (12) and (15), a least squares solution for minimum acceleration is obtained as:

$$(16) \quad \theta_{\Delta \min, a} = -(\mathbf{H}_{\theta_{\Delta}}^H \mathbf{W} \mathbf{H}_{\theta_{\Delta}} + \mathbf{R})^{-1} (\mathbf{H}_{\theta_{\Delta}}^H \mathbf{W} \mathbf{H} \mathbf{f})$$

### 3 NUMERICAL ANALYSIS AND RESULTS

The method has been applied to a light utility helicopter based on SA349/2 Aerospatiale Gazelle for which extensive numerical and experimental studies are available in literature. The general features are provided in Table 3. In this work, the model data from References [21], [22] and [20] are used.

Table 3: General features of SA349/2 helicopter

Main Rotor Radius	5.25 m
Number of Blades	3
Blade-Hub Connection	Articulated
Main Rotor Angular Speed	387 RPM
Mean Chord	33.6 cm
Max. Helicopter Mass	2000 kg
Maximum Speed	167 knots

A CAMRAD JA model of the SA342 Gazelle configuration has been built using the data in Ref. 22. The reliability of the model for 3/rev loads was studied and discussed in a previous work [23]. In helicopters, since the blade angle of attack and advancing airflow speed depend on the forward flight speed and, as the forward flight speed increases, the magnitude of oscillations in blade advancing airspeed increases, inducing a higher level of vibratory loads. Therefore the vibration level originating from the main rotor is theoretically zero at hover and increases with forward flight speed to high levels [24]. For this reason  $\mu = 0.30$  is selected as the representative flight condition in most of the rotorcraft vibration optimization studies [25]. Therefore hover condition and the low forward flight speeds are excluded and the analysis have been performed between the advance ratios  $\mu = 0.25$  and  $\mu = 0.40$  with an advance ratio increment of 0.05.

#### 3.1 Optimization for minimum vertical hub force at 3/rev

Table 4 gives the result of the optimization for vertical 3/rev force ( $F_z$ ) and the other force and moment components that are constrained with the limit values for each flight condition. The application of HHC reduces 3/rev vertical force ( $F_z$ ) by ap-

Table 4: Comparison of HHC-ON and HHC-OFF 3/rev Forces (N.) and Moments (Nm.)

Force- $\mu$	0.25	0.30	0.35	0.40
<i>Limit</i>	930	930	930	930
$F_x(OFF)$	82	65	113	367
$F_x(ON)$	58	41	123	353
$F_y(OFF)$	84	51	51	150
$F_y(ON)$	152	171	109	182
$F_z(OFF)$	2153	2593	3243	4945
$F_z(ON)$	1444	960	1935	4666
Moment- $\mu$	0.25	0.30	0.35	0.40
<i>Limit</i>	294	395	540	795
$M_x(OFF)$	97	138	294	785
$M_x(ON)$	250	363	460	846
$M_y(OFF)$	94	201	301	567
$M_y(ON)$	121	157	457	415
$M_z(OFF)$	298	384	577	1177
$M_z(ON)$	197	198	415	1045

proximately 30%, 59% and 40% for the advance ratios of 0.25, 0.30 and 0.35 respectively. At these advance ratios the constraints for the force and moment components other than vertical force are satisfied. In terms of the intended optimization, the flight condition with 0.40 advance ratio is the only unsuccessful case. It is believed that the level of complexity in the oscillatory airloads cannot be smoothed within the prescribed limit of HHC input, one degree magnitude, due to control power requirement considerations.

The required 3/rev HHC input in the non-rotating frame for the range of the HHC analysis are presented in Table 5. According to the limit value, the magnitude of these values should be less than one degree. The highest input magnitude is found to be 0.89 degrees at  $\mu = 0.30$  for collective input.

The results of the optimization are summarized in Figure 7. For the next analysis, since MASST requires an isolated rotor model, the results for both full helicopter model and isolated rotor models are provided for verification of isolated models. It can be concluded that both models give close results and show similar trend for initial and reduced loads in the prescribed range of advance ratio.

#### 3.2 Aeroservoelastic Analysis in MASST

Following the described method, a MASST aeroservoelastic model has been developed to investigate the airframe vibration reduction. The model is relatively simple but has all the features that are essential for rotor/fuselage coupled vibra-

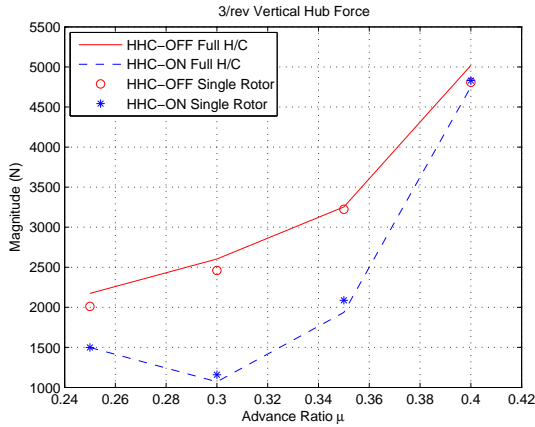


Figure 7: HHC ON and OFF Cases for full helicopter and isolated rotor models

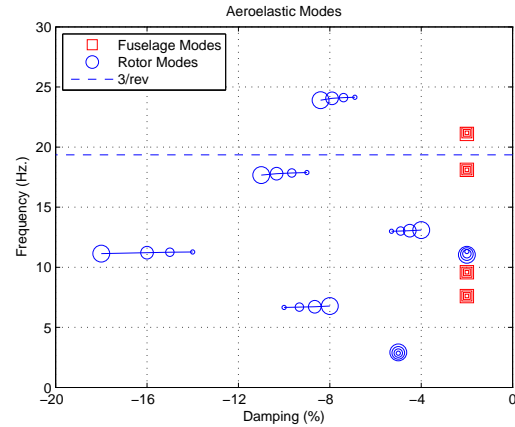


Figure 8: Aeroelastic modes, transition from 0.25 advance ratio to 0.40 with increasing marker size

tion problem of rotorcraft which include;

- Aeroelastic rotor model
- Elastic Gearbox support that supports the main rotor and transfers rotor loads
- Aeroelastic coupling between rotor and fuselage
- Rigid and elastic behaviour of the Fuselage Model covering the frequency of interest
- Sensors to measure the accelerations on the prescribed airframe locations
- Vibratory hub loads to excite the vehicle at the the frequency of interest
- Control chain from servo actuators to blades to input required HHC swashplate angles

Table 5: Optimal swashplate HHC inputs in non-rotating reference frame

$\mu$	Component	Cos.	Sin.
0.25	Collective	0.23	-0.14
	Longitudinal	0.18	-0.19
	Lateral	0.06	0.09
0.30	Collective	0.72	-0.52
	Longitudinal	0.28	-0.28
	Lateral	0.07	0.08
0.35	Collective	0.59	-0.33
	Longitudinal	0.14	-0.26
	Lateral	-0.24	0.05
0.40	Collective	0.06	0.10
	Longitudinal	0.07	-0.03
	Lateral	-0.02	-0.02

First, aeroelastic stability has been checked. The coupled rotor fuselage aeroelastic modes in the range of interest are given in Figure 8. The vehicle is concluded as aeroelastically stable since all aeroelastic roots appear on left hand side of complex plane, i.e negative real root. Since the analysis focuses on high frequencies, a stabilization system for rigid body modes was not included. The unstable rigid body modes, which are at zero or very low frequency and hence far below 3/rev, are rather removed from the system.

Vibrations in longitudinal, lateral and vertical direction have been computed at the sensor locations, previously reported in Table 1, to assess the amount of reduction in the magnitude of sensor acceleration in vertical ( $z$ ) direction and to observe the effects of minimization of vertical force in the accelerations in longitudinal ( $x$ ) and lateral ( $y$ ) directions. The HHC-OFF vibrations are compared to those of two HHC application strategies. The first one is the HHC-ON case using the HHC input obtained from minimum force optimization (labeled as min. F) and the other one is HHC-ON case obtained by least squares solution. For the least squares optimization two sets of analyses were performed with the same weight matrix  $\mathbf{W}$  of Eq. (9), in which, the weights are given as 1.00 for vertical acceleration and 0.25 for longitudinal and lateral accelerations in the diagonal element so that the vertical acceleration is given priority while the vibrations in other two directions are not allowed to change significantly.

Two sets of analysis were performed with the same weight matrix  $\mathbf{W}$ . First, since the optimization problem limits the magnitude of HHC input, for comparison of two objectives, the weighting matrix

$\mathbf{R}$  of Eq. (9) was adjusted accordingly using trial and error approach to give the maximum HHC input component as 1 deg (labeled as min a.). It is also possible to formulate control inputs in least squares solution as constraints rather than using the  $\mathbf{R}$  matrix. However for the intended aim of the analysis, a trial and error was found sufficient. For the second least squares solution,  $\mathbf{R}$  matrix was set to zero (labeled as min a. R=0) to investigate the maximum reduction and the cost of minimized cabin vibration.

For the advance ratio range considered in the analysis, the time history over one rotor revolution is given for one of the cases in Figure 9 for a representation of all cases. For the overall advance ratio range, the magnitudes of the sensor accelerations are compared in Figures 10, 11 and 12 in the  $x$ ,  $y$  and  $z$  directions respectively. Their corresponding magnitudes of HHC inputs are provided in Table 6. As postulated above, the results show that the reduction in  $N/rev$  loads also reduce the cabin vibrations. However, the plots show that the vibrations differ as the sensor location differ in the same advance ratio although the hub loads are unique for a given flight condition. Therefore, it is always more accurate to work with a fuselage model and formulate the reduction problem in terms of accelerations.

The effect of the minimum force optimization strategy and the different weights in matrix  $\mathbf{W}$  can be observed by comparing the acceleration in ( $x$ ), ( $y$ ) and ( $z$ ) directions of Figures 10, 11 and 12. As mentioned before the vibratory force in  $z$  direction is minimized while constraining other force and moment components below reference values for the minimum force objective and the weights in least squares formulation are higher in vertical direction as compared to the other two directions. Because of this reason, while the accelerations in  $z$  direction reduced for all the sensors at the whole advance ratio range, the accelerations in  $y$  and  $x$  directions after HHC actuation are sometimes lower sometimes higher as compared to that of reference HHC-OFF case. This is a trade off between the level of aimed reduction in critical direction(s) and the allowable margin of vibration increase in the other direction(s).

Another observation is that the least squares minimization gives lower acceleration magnitudes as compared to minimum force optimization. This is expected since the objective of least squares minimization is directly the accelerations at sensors. On the other hand the objective of the minimum force optimization considers the magnitude

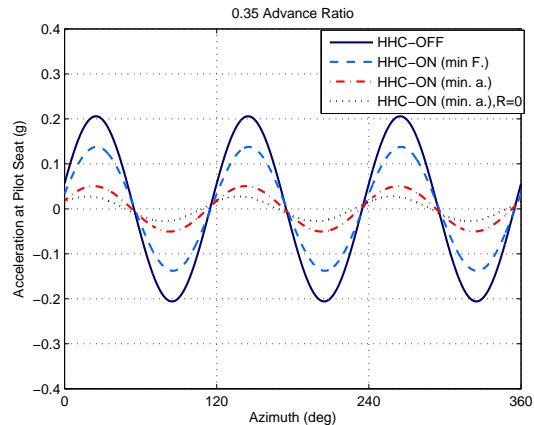


Figure 9: Comparison of time histories over one rotor revolution for the acceleration at 0.35 advance ratio at sensor # 2

of  $3/rev$  vertical force at hub and hence its effect on airframe acceleration reduction is on input level which means that the load path from the rotor to the sensors in the fuselage is not taken into account. Therefore it can be concluded that reduction in the vibratory hub loads means reduced vibrations in the airframe but does not necessarily lead to minimum vibrations.

Finally, the last columns of Figures 10, 11 and 12 give the possible minimum level of the sensor accelerations for the least squares formulation, i.e. the weighting matrix for control inputs ( $\mathbf{R}$ ) is zero. The cost of zero  $\mathbf{R}$  matrix can be observed from the values which have at least one of the components larger than 1 deg, as given in most right column of Table 6. These values can be considered as a maximum performance for cabin vibration reduction application. For this particular analysis, the maximum values are not significantly higher than those of the limited applications.

#### 4 CONCLUSIONS AND FUTURE WORK

Reduction in vibratory loads and vibrations by higher harmonic control active vibration control technique has been presented. Although being simple for a detailed vibration analysis, a stick model including a gearbox attachment that can provide all the essential features for vibration reduction has been developed. The objectives of minimum oscillatory hub loads and minimum acceleration on fuselage have been analyzed on comprehensive aeroelastic rotorcraft models. The vibratory loads and vibrations have been compared for the HHC-OFF and HHC-ON cases and

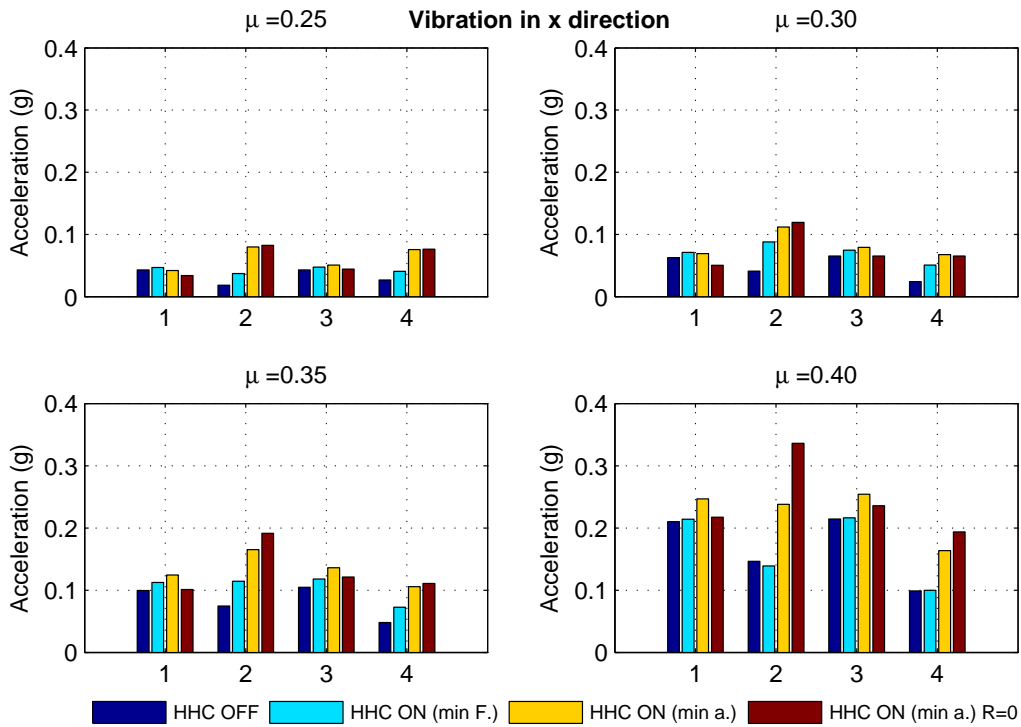


Figure 10: Magnitude of longitudinal sensor accelerations (labeled 1, 2, 3, 4) for HHC-OFF and HHC-ON inputs coming from minimum force optimization (min F.) and least squares acceleration minimization (min a.) and least squares acceleration minimization (min a.) without limit,  $\mathbf{R}=0$

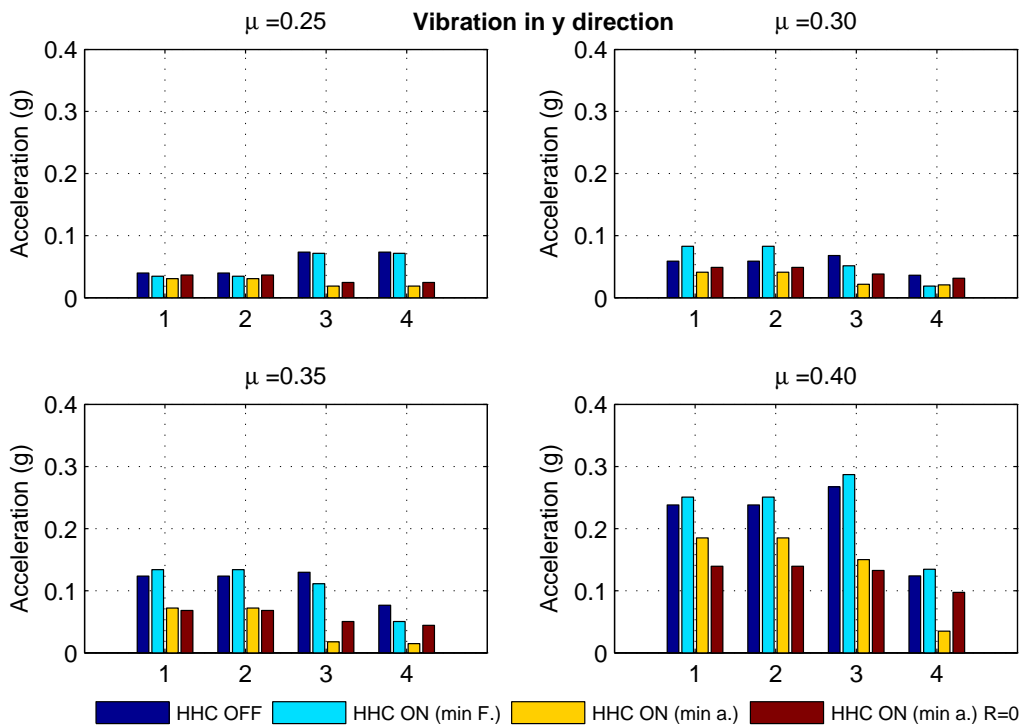


Figure 11: Magnitude of lateral sensor accelerations (labeled 1, 2, 3, 4) for HHC-OFF and HHC-ON inputs coming from minimum force optimization (min F.) and least squares acceleration minimization (min a.) and least squares acceleration minimization (min a.) without limit,  $\mathbf{R}=0$

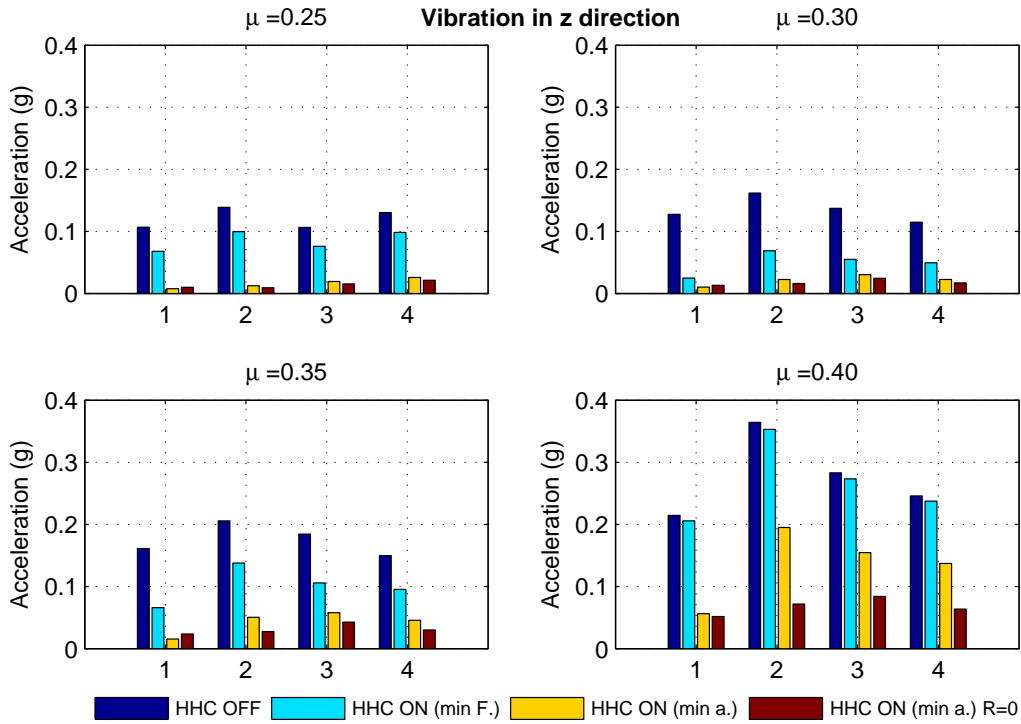


Figure 12: Magnitude of vertical sensor accelerations (labeled 1, 2, 3, 4) for HHC-OFF and HHC-ON inputs coming from minimum force optimization (min F.) and least squares acceleration minimization (min a.) and least squares acceleration minimization (min a.) without limit,  $\mathbf{R}=0$

results have been discussed.

This study proves that MASST aeroservoelastic analysis tool is efficient in active vibration control analysis. In addition to analysis capability, an integrated aeroelastic rotor model capable of providing aeroelastic model together with harmonic rotor loading is expected to convert it to a novel design tool. With the rotor addition, sensitivities and

robustness of an objective to design parameters can be easily included in active vibration control design.

#### ACKNOWLEDGMENTS

This work is an extension of the collaboration between Middle East Technical University and TAI (Turkish Aerospace Industries). The unpublished rotor optimization study was conducted at the time of collaboration using CAMRAD JA software of TAI. The authors gratefully acknowledge the permission given.

Table 6: Magnitude of swashplate HHC inputs

$\mu$	Comp.	$\theta_{\Delta, min_F}$	$\theta_{\Delta, min_a}$	$\theta_{\Delta, min_a-R0}$
0.25	Col.	0.27	0.69	0.84
	Long.	0.27	0.40	0.39
	Lat.	0.13	1.00	1.09
0.30	Col.	0.89	0.80	1.17
	Long.	0.40	0.28	0.11
	Lat.	0.11	1.00	1.17
0.35	Col.	0.68	0.74	1.31
	Long.	0.30	0.57	0.44
	Lat.	0.25	1.00	1.26
0.40	Col.	0.12	0.61	1.69
	Long.	0.08	0.72	1.87
	Lat.	0.03	1.00	1.40

#### REFERENCES

- [1] Pierangelo Masarati, Giuseppe Quaranta, Massimo Gennaretti, and Jacopo Serafini. An investigation of aeroelastic rotorcraft-pilot interaction. In *37th European Rotorcraft Forum*, Gallarate, Italy, September 13–15 2011. Paper no. 112.
- [2] Giuseppe Quaranta, Aykut Tamer, Vincenzo Muscarello, Pierangelo Masarati, Massimo Gennaretti, Jacopo Serafini, and Marco Molica Colella. Evaluation of rotorcraft aeroelastic stability using robust analysis. In *38th European Rotorcraft Forum*, Amsterdam, NL, 2012.
- [3] Giuseppe Quaranta, Aykut Tamer, Vincenzo Muscarello, Pierangelo Masarati, Massimo Gennaretti, Jacopo Ser-

- afini, and Marco Molica Colella. Rotorcraft aeroelastic stability using robust analysis. *CEAS Aeronaut. J.*, in press, 2013.
- [4] Kristin L. Harrer, Debra Yniguez, Maria Majar Maria, David Ellenbecker, Nancy Estrada, and Mark Geiger. Whole body vibration exposure for MH-60s pilots. In *43th SAFE*, Utah, USA, 2005.
- [5] A. R. S. Bramwell. *Helicopter Dynamics*. Edward Arnold, London, 1976.
- [6] Rendy P. Cheng, Mark B. Tischler, and Roberto Celi. A high-order, linear time-invariant model for application to higher harmonic control and flight control system interaction. TR 04-005, NASA, 2006.
- [7] A.C. VECA. Vibration effects on helicopter reliability and maintainability. TM 73-11, NASA, 1973.
- [8] M.N.H. Hamouda and G.A. Pierce. Helicopter vibration suppression using simple pendulum absorbers on the rotor blade. CR NSG-1592, NASA, 1982.
- [9] K.Q. Nguyen. Higher harmonic control analysis for vibration reduction of helicopter systems. TM 103855, NASA, 1994.
- [10] Richard L. Bielawa. *Rotary Wing Structural Dynamics and Aeroelasticity*. AIAA, Washington, DC, 2005.
- [11] Lawson H. Robinson and Peretz P. Friedmann. A study of fundamental issues in higher harmonic control using aeroelastic simulation. *Journal of the American Helicopter Society*, pages 32–43, 1991.
- [12] S.S. Rao. *Engineering Optimization*. John Wiley & Sons, 1996.
- [13] Wayne Johnson. *CAMRAD/JA, A Comprehensive Analytical Model of Rotorcraft Aerodynamics and Dynamics, Johnson Aeronautics Version*. Johnson Aeronautics, 1988.
- [14] G.N. Vanderplaats. Conmin - a fortran program for constrained function minimization users manual. TM 62282, NASA, 1973.
- [15] Pierangelo Masarati, Vincenzo Muscarello, and Giuseppe Quaranta. Linearized aeroservoelastic analysis of rotary-wing aircraft. In *36th European Rotorcraft Forum*, pages 099.1–10, Paris, France, September 7–9 2010.
- [16] Pierangelo Masarati, Vincenzo Muscarello, Giuseppe Quaranta, Alessandro Locatelli, Daniele Mangone, Luca Riviello, and Luca Viganò. An integrated environment for helicopter aeroservoelastic analysis: the ground resonance case. In *37th European Rotorcraft Forum*, pages 177.1–12, Gallarate, Italy, September 13–15 2011.
- [17] Roy R. Craig, Jr. and Mervyn C. C. Bampton. Coupling of substructures for dynamic analysis. *AIAA Journal*, 6(7):1313–1319, July 1968.
- [18] Gian Luca Ghiringhelli, Pierangelo Masarati, and Paolo Mantegazza. A multi-body implementation of finite volume beams. *AIAA Journal*, 38(1):131–138, January 2000. doi:10.2514/2.933.
- [19] Aykut Tamer and Pierangelo Masarati. Linearized structural dynamics model for the sensitivity analysis of helicopter rotor blades. In *Ankara International Aerospace Conference*, Ankara, TR, September 11–13 2013.
- [20] R.M. Heffernan and M. Gaubert. Vibration analysis SA349/2 helicopter. TM 102794, NASA, 1991.
- [21] R.M. Heffernan and M. Gaubert. Hub and blade structural measurements of an sa349/2 helicopter. TM 88370, NASA, 1986.
- [22] G.K. Yamauchi, R.M. Heffernan, and M. Gaubert. Structural and aerodynamic loads and performance measurements of an sa 349/2 helicopter with an advanced geometry rotor. TM 101040, NASA, 1988.
- [23] A. Tamer. Analysis and design of helicopter rotor blades for reduced vibrational level. Master's thesis, Middle East Technical University, Ankara, Turkey, 2011.
- [24] Wayne Johnson. *Helicopter Theory*. Princeton University Press, Princeton, New Jersey, 1980.
- [25] Peretz P. Friedmann. Helicopter vibration reduction using structural optimization with aeroelastic/multidisciplinary constraints — a survey. *J. Aircraft*, 28(1):8–21, 1991.